The Ultra-Wide Bandwidth Indoor Channel: From Statistical Model to Simulations

Dajana Cassioli, *Student Member, IEEE*, Moe Z. Win, *Senior Member, IEEE*, and Andreas F. Molisch, *Senior Member, IEEE*

***Abstract*—We establish a statistical model for the ultra-wide bandwidth (UWB) indoor channel based on an extensive measurement campaign in a typical modern office building with 2-ns delay resolution. The approach is based on the investigation of the statistical properties of the multipath profiles measured in different rooms over a finely spaced measurement grid. The analysis leads to the formulation of a stochastic tapped-delay-line (STDL) model of the UWB indoor channel. The averaged power delay profile can be well-modeled by a single exponential decay with a statistically distributed decay constant. The small-scale statistics of path energy gains follow Gamma distributions whose parameters m are truncated Gaussian variables with mean values and standard deviations decreasing with delay. The total received energy experiences a lognormal shadowing around the mean energy given by the path-loss power law. We also find that the correlation between multipath components is negligible. Finally, we propose an implementation of the STDL model and give a comparison between the experimental data and the simulation results.**

***Index Terms*—Propagation channel, stochastic tapped-delay line model, ultra-wide bandwidth.**

I. Introduction

ULTRA-WIDE bandwidth (UWB) spread-spectrum techniques have recently attracted great interest in scientific, commercial, and military sectors [1]–[13]. UWB signals are often defined as having 3-dB bandwidth greater than 25% of their center frequencies of the radiation [4], [14]. Recent results indicate that UWB radio is a viable candidate for short-range multiple-access communications in dense multipath environments, exploiting the advantages of the UWB-radio's fine delay resolution properties [15], [16]. Commonly, these radios [1]–[3] communicate with trains of short duration pulses with a low duty-cycle. By appropriately designing the multiuser access, it is possible to achieve multiuser-interference/inter-symbol-interference-resilient UWB transmission using linear receivers [9]. Recent efforts in reducing the receiver complexity [10], [17]–[19] make us envisage a wide diffusion of the UWB-radio technology.

The potential strength of the UWB-radio technique lies in its use of extremely wide transmission bandwidths, resulting in the following desirable capabilities including: 1) accurate position location and ranging, and lack of significant multipath fading due to fine delay resolution; 2) multiple access due to wide transmission bandwidths; 3) covert communications due to low transmission power operation; and 4) possible easier material penetration due to low frequency components. However, the UWB technology is not yet fully developed, and the efficient design of such communication systems requires new experimental and theoretical activities. In particular, an appropriate channel model that accurately describes the UWB propagation, yet is simple enough to enable tractable analysis and computer simulations is needed. Such a model has not been available up to now.

Many propagation measurements have been performed for indoor narrowband channels and several models have been proposed in the literature [20]–[23].[1] However, due to their restriction on measurement bandwidth, they were inadequate for the UWB system studies. Even the model in [20] is based on measurements made by probing the channels with only 10-ns pulses at 1.5 GHz. In this paper, we present a statistical analysis of the data collected from a UWB propagation experiment, performed in a typical modern office building with 2-ns delay resolution using baseband pulses [24]. The approach is based on the investigation of the statistical properties of the multipath profiles measured in different rooms over a finely spaced measurement grid. We analyze this data to arrive at a model for the UWB channel. Our modeling concept is based on well-validated approaches, like the ones proposed in [20], [21], and [25]. However, some important modifications are made to account for the special properties specific to UWB transmission.

Previous analyses of UWB systems in multipath environments use narrowband channel models or straightforward extensions to finer delay resolutions. For example, [8] uses the model of [20] as well as a deterministic two path model, and [11] uses an extension of the Δ–K model [22], [23], [26], to a delay resolution of 5 ns. More generally, performance analyses of UWB systems are usually based on channel models that imply Rayleigh fading. However, our analysis shows that the empirical distribution of the path gains markedly differs

Manuscript received April 3, 2001; revised October 18, 2001. This paper was presented in part at the IEEE VTS 53rd Vehicular Technology Conference, May 2001, Rhodos, Greece. The work of A. F. Molisch was supported by the Austrian Ministry of Science, the TU Wien, and the Oesterreichische Forschungsgemeinschaft.

D. Cassioli is with the Dipartimento di Ingegneria Elettronica, Università degli Studi di Roma "Tor Vergata," 00133 Roma, Italy (e-mail: cassioli@ing.uniroma2.it).

M. Z. Win is with the Wireless Systems Research Department, AT&T Labs–Research, Middletown, NJ 07748-4801 USA (e-mail: win@ieee.org).

A. F. Molisch was with the Institut fuer Nachrichtentechnik und Hochfrequenztechnik, Technische Universität Wien, A-1040 Vienna Austria. He is now with the Wireless Systems Research Department, AT&T Labs–Research, Middletown, NJ 07748-4801 USA (e-mail: Andreas.Molisch@ieee.org).

Publisher Item Identifier 10.1109/JSAC.2002.801228.

[1]In mobile radio communications, it is common to define "narrowband" as transmission bandwidth being much smaller than the coherence bandwidth of the channel. However in this paper, we use the RF engineering definition of narrowband, which is defined as the measurement bandwidth being much smaller than the carrier frequency.

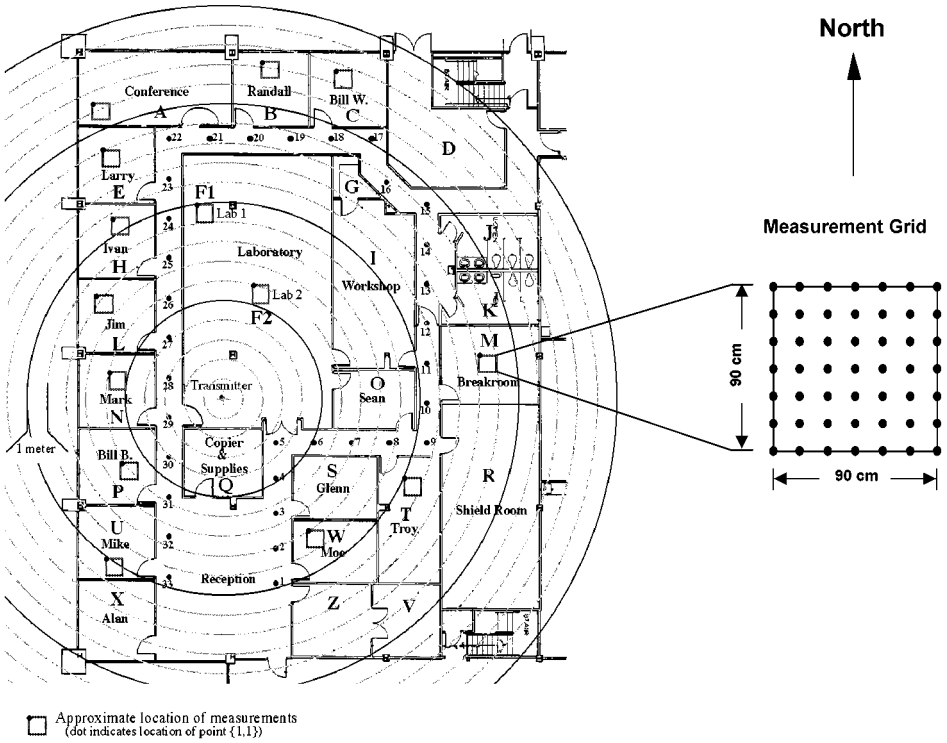

Fig. 1. The floor plan of a typical modern office building where the propagation measurement experiment was performed. The concentric circles are centered on the transmit antenna and are spaced at 1-m intervals.

from the exponential power statistics (i.e., Rayleigh amplitude statistics). This is due to the fact that UWB systems provide high resolution in the delay domain, implying that only a small number of multipath components (MPCs) fall within an interval of delay resolution.[2]

In this paper, we propose a stochastic tapped-delay-line (STDL) propagation model for the UWB indoor channel. All the parameters of the STDL model have been extracted from a set of measured impulse responses. Although the presented parameterization of the model is related to the particular building in which the propagation experiment was performed, the methodology can be adopted to interpret other similar sets of UWB experimental data. Furthermore, the proposed model is suitable to implement computer simulations of a generic UWB system operating in a typical indoor environment.

The paper is organized as follows. In Section II, the UWB propagation experiment is presented. The procedure by which we processed the experimental data to obtain a set of power delay profiles is described in Section III, along with the best fit procedures that are used to extract the model parameters. In Section IV, we developed the statistical model based on these parameters. Finally, in Section V, the simulation results generated based on our proposed model are discussed and compared with the experimental data. Conclusions are given in Section VI.

II. The UWB Propagation Experiment

Although our purpose here is to concentrate on the statistical analysis and the modeling of the channel rather than on the experiment itself, for the convenience of the reader, we give a review of the UWB propagation experiment that closely follows [24].

[2]The resolution of the signal is proportional to the inverse of the bandwidth.

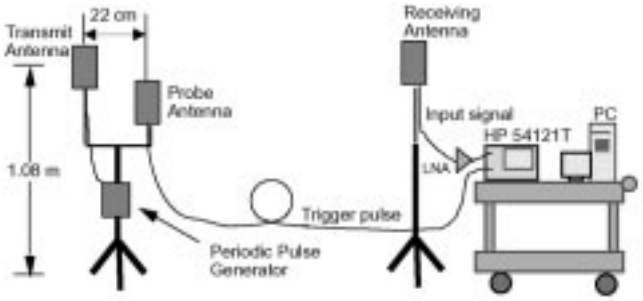

Fig. 2. A block diagram of the measurement apparatus.

A UWB propagation experiment was performed in a modern laboratory/office building having the floor plan shown in Fig. 1. The measurement technique employed in this measurement campaign is to probe the channel periodically with nanosecond pulses and to record its response using a digital sampling oscilloscope (DSO).

A diagram of the measurement apparatus is shown in Fig. 2. The UWB antennas, which are flat and roughly the size of a playing card, display nearly circularly symmetric patterns about their vertical axes. One of the three UWB antennas is set in close proximity to the transmit antenna to supply a trigger signal to the DSO over a long coaxial cable of fixed length. Therefore, all recorded multipath profiles have the same absolute delay reference, and delay measurements of the signals arriving to the receiving antenna via different propagation paths can be made. During each of the multipath profile measurements, both the transmitter and receiver are kept stationary.

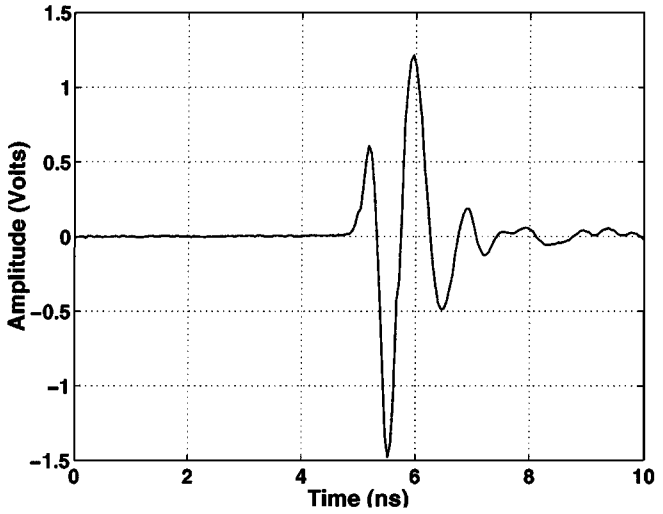

Fig. 3. The transmitted pulse measured by the receiving antenna located 1 m away from the transmitting antenna with the same height.

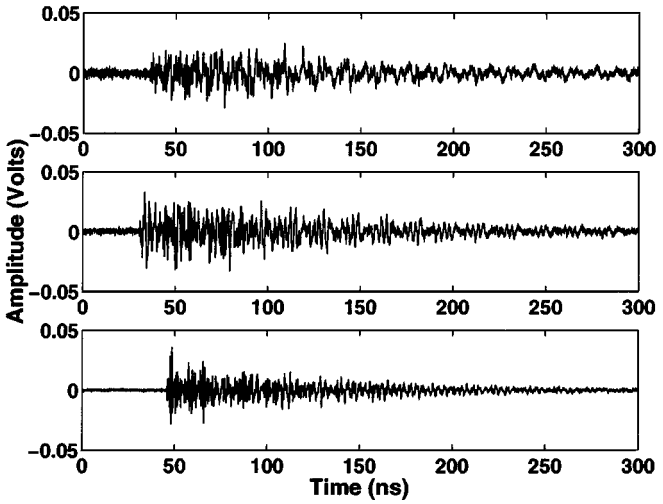

Fig. 4. Average multipath measurements of 32 sequentially measured multipath profiles where the receiver is located at the same exact locations in offices U (upper trace), W (middle trace), and M (lower trace). The measurement grids are 10, 8.5, and 13.5 m away from the transmitter, respectively.

The transmitted waveform, measured by the receiving antenna placed 1 m away from the transmitting antenna with the same height, is shown in Fig. 3. The repetition rate of the pulses is 2×10^6 pulses per second, implying that multipath spreads up to 500 ns could have been observed unambiguously. Multipath profiles with a duration of 300 ns were measured (Fig. 4). Multipath profiles were measured at various locations (see Fig. 1) in 14 rooms and hallways on one floor of the building. Each of the rooms is labeled alpha numerically. Walls around offices are framed with metal studs and covered with plaster board. The wall around the laboratory is made from acoustically silenced heavy cement block. There are steel core support pillars throughout the building, notably along the outside wall and two within the laboratory itself. The shield room's walls and door are metallic. The transmitter is kept stationary in the central location of the building near a computer server in a laboratory denoted by F. The transmit antenna is located 165 cm from the floor and 105 cm from the ceiling.

In each receiver location, impulse response measurements were made at 49 measurement points, arranged in a fixed-height, 7×7 square grid with 15-cm spacing, covering 90 cm $\times$ 90 cm. A total of 741 different impulse responses were recorded. One side of the grid is always parallel to north wall of the room. The receiving antenna is located 120 cm from the floor and 150 cm from the ceiling.

Profiles measured over in offices U, W, and M are shown in Fig. 4. The approximate distances between the transmitter and the locations of these measurements are 10, 8.5, and 13.5 m, respectively. Fig. 4 also shows that the response to the first probing pulse has decayed almost completely in roughly 200 ns, and has disappeared before the response to the next pulse arrives at the antenna. The multipath profiles recorded in the offices W and M have a substantially lower noise floor than those recorded in office U. This can be explained, with the help of Fig. 1, by observing that office U is situated at the edge of the building with a large glass window and is subject to more external interference (e.g., from radio stations, television stations, cellular and paging towers), while offices W and M are situated roughly in the middle of the building. In general, an increased noise floor was observed for all the measurements made in offices located at edges of the building with large glass windows.

III. Data Processing and Analysis Results

We processed all the multipath profiles measured in the 14 rooms and obtained 14 $\times$ 49 different power delay profiles (PDPs). We separately analyze the effects of the *large* and *small* scale fading statistics. The large-scale fading characterizes the changes in the received signal when the receiver position varies over a significant fraction of the transmitter–receiver (T–R) distance and/or the environment around the receiver changes. This situation typically occurs when the receiver is moved from one room to another room in a building.[3] The small-scale effects, on the other hand, are manifested in the changes of the PDP caused by small changes of the receiver position, while the environment around the receiver does not change significantly. This occurs, for instance, when the receiver is moved over the measurement grid within a room in a building.

In the following, we refer to the PDP measured at one of the 14 $\times$ 49 locations as *local* PDP, while we denote the PDP averaged over the 49 locations within one room as the *small-scale averaged* PDP (SSA-PDP). This spatial averaging (mostly) removes the effect of small-scale fading. The small-scale statistics are derived by considering the deviations of the 49 local PDPs from the respective SSA-PDP. The large-scale fading may be investigated by considering the variation of the SSA-PDPs over the different rooms. We also make a distinction between the "local" parameters, which refer to the small-scale effects, and the "global" parameters, extracted from the SSA-PDPs. For clarity, all the symbols and parameters are listed in Table I.

[3]There could also be large-scale changes within one room if it is large enough. However, with our measurement setup and choice of measurement points, this effect could not be observed. It is also possible that some of the 49 measurement points within one room were shadowed. However, it was not possible to separate this effect from the small-scale fading (see also Section V).

TABLE I
SYMBOLS AND PARAMETERS

DELAY AXIS	
τ	Excess Delay
τ_{Ref}	Absolute Propagation Delay
$\tau_k = (k-1)\Delta\tau$	k^{th} Delay Bin
$\Delta\tau = 2\ ns$	Bin Width
N_{bins}	Number of Bins
ENERGY GAINS	
$\overline{G}_{\text{tot}}$	Total Average Energy Gain
$\overline{G}_k$	Average Energy Gain of the k^{th} Delay Bin
G_k	Energy Gain of the k^{th} Delay Bin
$\overline{g}(\tau)$	Average Received Energy at Excess Delay τ
EXPONENTIAL TIME DECAY	
ε	Decay Constant
$r = G_2/G_1$	Power Ratio

Since the absolute propagation delays of the received signals vary from one location to another, an appropriate delay reference is needed to characterize the relative delays of each resolved MPC. We take the reference τ_{Ref} as the absolute propagation delay, i.e., the delay of the direct or quasi-line-of-sight (LOS) path given according to the geometry: $\tau_{\text{Ref}} = d/c$, where d is the T–R separation distance and c is the speed of light. We then translate the delay axis of the measured multipath profiles for each location by its respective τ_{Ref}.

As in [21], the delay axis is quantized into bins, and the received power is integrated within each bin to obtain the local PDP in terms of the pairs $\{G_k, \tau_k\}$, where G_k is the energy gain defined as the ratio between the energy received at a T–R distance d, over a bin width $\Delta\tau$ beginning at the delay $\tau_k = (k-1)\Delta\tau$, and the total energy received at the reference distance of one meter.[4] We chose the widths of the bins to be $\Delta\tau = 2$ ns. This value is a good compromise between high delay resolution, and reduction of the effects of noise and imperfect back-to-back calibration.

To reduce the noise, we set the power of all the bins below a threshold to zero. The threshold was set to be 6 dB [27] above the noise floor, which is defined as the average noise energy within one delay bin. The noise floor for each room is computed separately, namely by computing the energies per bin from the portion of the PDP that is measured *before* the first multipath component arrives (i.e., before τ_{Ref}), and averaging these energies over the 49 locations within a room.

A. The Large-Scale Statistics

All SSA-PDPs exhibit an exponential decay as a function of the excess delay. Since we perform a delay axis translation, the direct path always falls in the first bin in all the PDPs.[5] It also turns out that the direct path was always the strongest path in the 14 SSA-PDPs even if the LOS is obstructed. The energy of the subsequent MPCs decay exponentially with delay starting from the second bin. This is illustrated by the fit (linearly on a decibel scale) in Fig. 5 using the SSA-PDP of a typical high signal-to-noise ratio (SNR) room. Let $\overline{G_k} \triangleq \mathbb{A}_{\text{Spa}}\{G_k\}$ be the locally averaged energy gain, where the $\mathbb{A}_{\text{Spa}}\{\cdot\}$ denotes the spatial average over the 49 locations of the measurement grid. The average energy of the second MPC may be expressed as a fraction r of the average energy of the direct path, i.e., $r = \overline{G}_2/\overline{G}_1$. We refer to r as the *power ratio.* As we will show in Section IV, the SSA-PDP is completely characterized by $\overline{G}_1$, the power ratio r, and the decay constant ε (or equivalently, by the total average received energy $\overline{G}_{\text{tot}}$, r, and ε).[6] The number of resolved MPCs is given by the number of the MPCs that exceed the threshold discussed above and, thus, given the threshold, it depends on the shape of the SSA-PDP, characterized by the parameters $\overline{G}_1$, r, and ε. We performed best-fit procedures to extract the ε's and the r's from the SSA-PDP of each room.

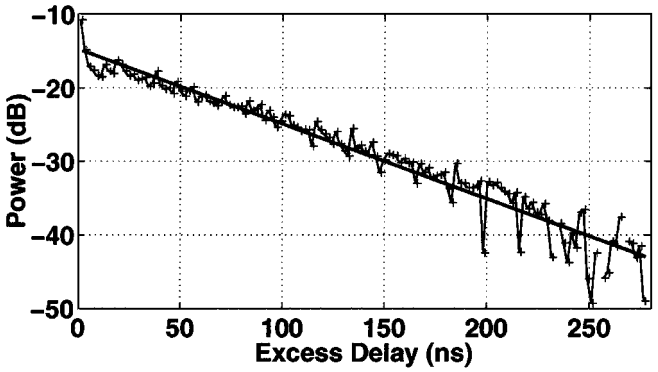

Fig. 5. The average power delay profile versus the excess delay in a semi-logarithmic scale for a typical high SNR room. The wavy line is the measured profile, the straight line is the exponential decay obtained by a best fit procedure.

The power ratio r and the decay constant ε vary from location to location, and we treat them as stochastic variables. As only 14 values for ε and r were available, it was not possible to extract the *shape* of their distribution from the measurement data. Instead, we assumed a model *a priori* and fitted the *parameters* of this distribution. Previous narrowband studies showed that the decay constants are well modeled as lognormal variates [28]. We found that the lognormal distribution, denoted by $\varepsilon \sim \mathcal{L}_{\mathcal{N}}(\mu_{\varepsilon_{\text{dB}}}; \sigma_{\varepsilon_{\text{dB}}})$, with $\mu_{\varepsilon_{\text{dB}}} = 16.1$ and $\sigma_{\varepsilon_{\text{dB}}} = 1.27$ gives the best agreement with the empirical distribution.[7] The histograms of the experimental decay constants and the theoretically-fitted distribution are shown in Fig. 6. Applying the same

[4]Here and throughout the paper, energies are normalized to the total energy received at 1-m distance.

[5]According to the bin's width in the delay domain, we can only resolve the MPCs arriving at differential delay greater than 2 ns. Thus, even if more than one path arrives within the bin, we refer to the content of each bin as one MPC.

[6]This is due to the fact that $\overline{G}_{\text{tot}}$ is related to $\overline{G}_1$, r, and ε, see Section IV.

[7]To be more precise, we converted the decay constants to a dB scale with reference value 1 ns, i.e., $\varepsilon_{\text{dB}} = 10\log_{10}(\varepsilon/1\text{ ns})$, and fitted those logarithmic decay constants to a normal distribution. We found that normal distribution with mean 16.1 and standard deviation 1.27 gave the best fit. In the following, we will abbreviate this by saying that the decay constant is distributed lognormally, $\varepsilon \sim \mathcal{L}_{\mathcal{N}}(\mu_{\varepsilon_{\text{dB}}};\ \sigma_{\varepsilon_{\text{dB}}})$ with mean $\mu_{\varepsilon_{\text{dB}}} = 16.1$, $\sigma_{\varepsilon_{\text{dB}}} = 1.27$.

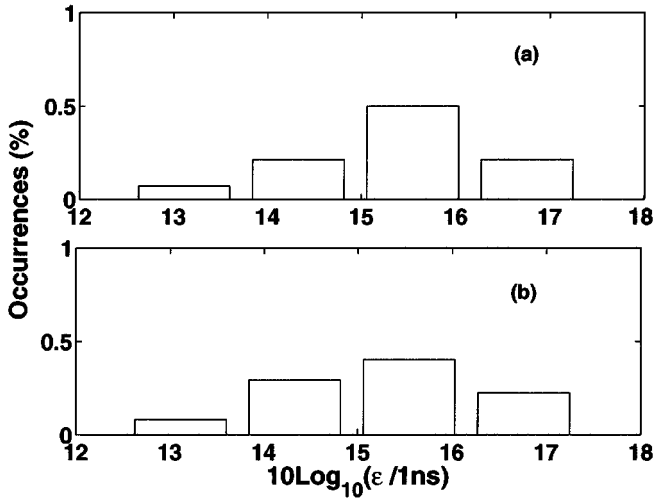

Fig. 6. Histograms of (a) the experimental decay constants ε and of (b) the theoretically fitted distribution. The decay constants are expressed in logarithmic units by referring to nanoseconds.

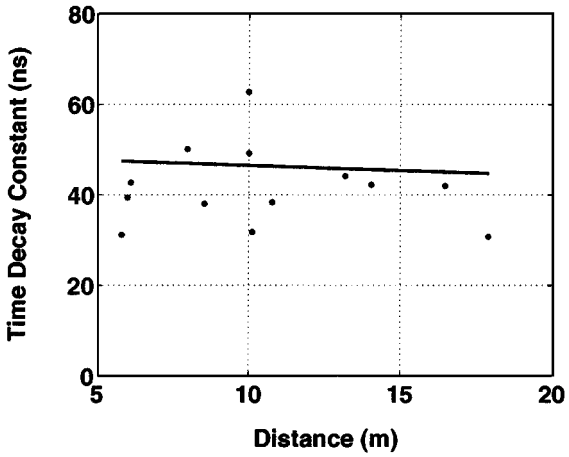

Fig. 7. Scatter plot of the decay constants ε versus the T–R distance. The solid line is the regression fit whose slope is -0.22 ns/m.

procedure to characterize the power ratios r's, we found that they are also lognormally distributed, i.e., $r \sim \mathcal{L}_{\mathcal{N}}(\mu_{r_{\rm dB}};\, \sigma_{r_{\rm dB}})$ with $\mu_{r_{\rm dB}} = -4$ $\sigma_{r_{\rm dB}} = 3$, respectively.[8]

We also investigated the possible correlation of the decay constant with the T–R separation, by applying a linear regression to the ε's versus the distance. As Fig. 7 shows, the regression fit of the decay constants ε's decreases with the increasing distance so slightly that we can conclude that it is *de facto* independent.

By integrating the SSA-PDP of each room over all delay bins, we obtained the total average energy $\overline{G}_{\rm tot}$ within each room. We then analyzed its dependence on the T–R separation. As suggested by the scatter plot of Fig. 8, we adopt a breakpoint model, commonly referred to as *dual slope* model, for path loss PL as a function of the distance. The regression lines are shown

[8]Since the r values are already ratios, their representation on a logarithmic scale is straightforward, $r_{\rm dB} = 10\log(r)$. Again, the histogram of the $r_{\rm dB}$ can be fitted by a normal distribution, now with mean -4 and standard deviation 3.

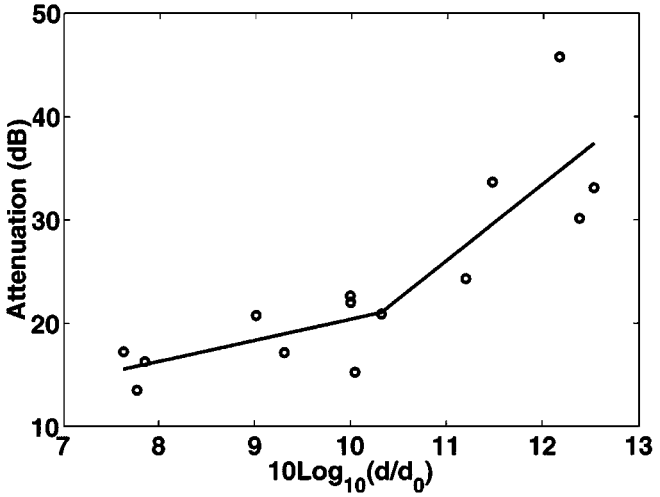

Fig. 8. Scatter plot of the large-scale attenuation versus the logarithm of the distance. The solid line represents the best fit with the path-loss model of (1).

in Fig. 8 and the parameters extracted by performing a best fit of the empirical attenuation are

$$PL = \begin{cases} 20.4 \cdot \log_{10}(d/d_0), & d \le 11 \text{ m} \\ -56 + 74 \cdot \log_{10}(d/d_0), & d > 11 \text{ m} \end{cases} \quad (1)$$

where PL is expressed in decibels, $d_0 = 1$ m is the reference distance, and d is the T–R separation distance in meters. Because of the shadowing phenomenon, the $\overline{G}_{\rm tot}$ varies statistically around the value given by (1). A common model for shadowing is lognormal distribution [28], [29]. By assuming such a model, we found that $\overline{G}_{\rm tot}$ is lognormally distributed about (1) with a standard deviation of the associated normal random variable equal to 4.3.[9]

B. The Small-Scale Statistics

The differences between the PDPs at the different points of the measurement grid are caused by the small-scale fading. In "narrowband" models, it is usually assumed that the magnitude of the first (quasi-LOS) multipath component follows Rician or Nakagami statistics and the later components are assumed to have Rayleigh statistics [30]. However, in UWB propagation each resolved MPC is due to a small number of scatterers, and the amplitude distribution in *each* delay bin differs markedly from the Rayleigh distribution.

In fact, the presented analysis showed that the best-fit distribution of the small-scale magnitude statistics is the Nakagami distribution [31], corresponding to a Gamma distribution of the energy gains. This distribution has been used to model the magnitude statistics in mobile radio when the conditions of the central limit theorem are not fulfilled [32].

We characterize the small-scale statistics by fitting the received normalized energies $\{G_k^{(i)}\}$ in *each* bin at the 49 locations of the measurement grid to a distribution.[10] The variations over the measurement grid are treated as stochastic. The result

[9]Again, we are considering the logarithm of the path loss, which is already a ratio (of total received energies at distances of d and 1 meters), so that the lognormal distribution can be interpreted analogously to the one for r.

[10]In the notation $G_k^{(i)}$, the subscript k indicates the kth bin at delay τ_k, while the superscript i indicates the ith location on the grid.

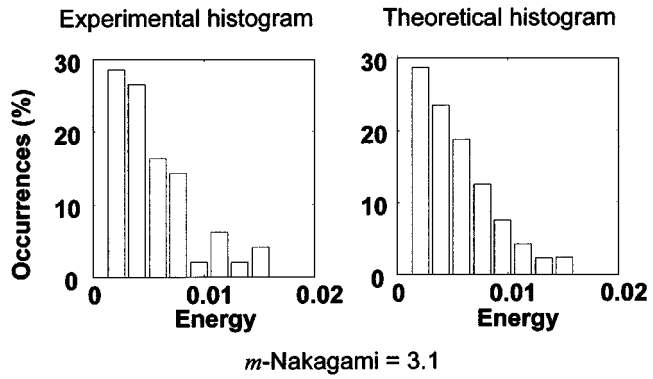

Fig. 9. Histogram of the received energy in the 34th bin of a typical high-SNR room, compared with the theoretical Gamma distribution, whose mean Ω_{34} and m_{34} were extracted from the experimental PDP. The energies on the horizontal axes are expressed in arbitrary units.

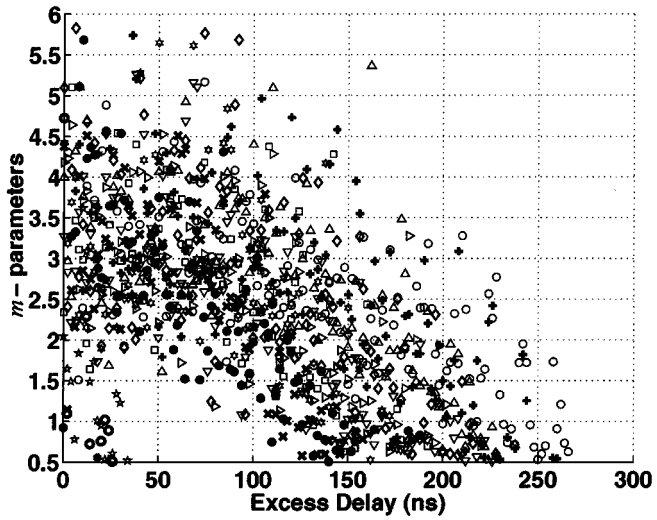

Fig. 10. Scatter plot of the m-Nakagami of the best fit distribution versus excess delay for all the bins except the LOS components. Different markers correspond to measurements in different rooms.

shows that the statistics of the energy gain vary with delays. Let us denote with $\Gamma(\Omega;\, m)$ the Gamma distribution with parameters Ω and m. The $\Gamma(\Omega; m)$ gives a good fit of the empirical distribution of the energy gains. The accuracy of the fit has been quantified in terms of the relative mean-squared error, which varies between 0.0105 (for the highest SNR) to 0.1137 (for the lowest SNR). A comparison between experimental and theoretical histograms for one exemplary bin in a typical high SNR is shown in Fig. 9.

The parameters of the Gamma distribution vary from bin to bin: $\Gamma(\Omega_k;\, m_k)$ denotes the Gamma distribution that fits the energy gains of the local PDPs in the kth bin within each room. The Ω_k are given as $\Omega_k = \overline{G}_k$, i.e., the magnitude of the SSA-PDP in the kth bin. The m_k are related to the variance of the energy gain of the kth bin. Fig. 10 shows the scatter plot of the m_k as a function of excess delay for all the bins (except the LOS components). It can be seen from Fig. 10 that the m_k values range between 1 and 6 (rarely 0.5), decreasing with the increasing excess delay. This implies that MPCs arriving with large excess delays are more diffused than the first arriving components, which agrees with intuition.

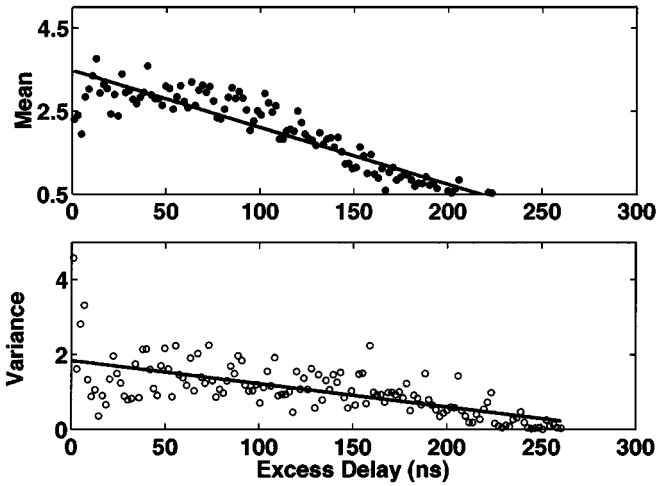

Fig. 11. Scatter plot of the mean values (dots) and the variance (circles) of the Gaussian distributions that fit the experimental distribution of m values at each excess delay. The solid lines represent the linear regression for these parameters, respectively.

The m_k parameters of the Gamma distributions themselves are random variables distributed according to a truncated Gaussian distribution, denoted by $m \sim \mathcal{T}\mathcal{N}(\mu_m; \sigma_m^2)$, i.e., their distribution looks like a Gaussian for $m \geq 0.5$ and zero elsewhere

$$f_m(x) = \begin{cases} K_m e^{-((x-\mu_m)^2/2\sigma_m^2)}, & \text{if } x \geq 0.5 \\ 0, & \text{otherwise} \end{cases} \tag{2}$$

where the normalization constant K_m is chosen so that the integral over the $f_m(x)$ is unity. Fig. 11 shows the mean and variance of such Gaussian distributions that fits the m_k as a function of the excess delay, along with the respective regression lines. The regression lines are given by

$$\mu_m(\tau_k) = 3.5 - \frac{\tau_k}{73} \tag{3}$$

$$\sigma_m^2(\tau_k) = 1.84 - \frac{\tau_k}{160} \tag{4}$$

where the unit of τ_k is in nanoseconds.

C. Correlation of MPCs Among Different Delay Bins

We next evaluate the correlation between the energy gain of the MPCs arriving in the same room at different excess delays as

$$\rho_{k,\,k+m} = \frac{\mathbb{A}_{\text{Spa}}\left\{\left(G_k - \overline{G_k}\right)\left(G_{k+m} - \overline{G_{k+m}}\right)\right\}}{\sqrt{\mathbb{A}_{\text{Spa}}\left\{\left(G_k - \overline{G_k}\right)^2\right\}\mathbb{A}_{\text{Spa}}\left\{\left(G_{k+m} - \overline{G_{k+m}}\right)^2\right\}}}.$$

The analysis shows that the correlation coefficients remain below 0.2 for almost all rooms and delay bins and is, thus, negligible for all practical purposes. This allows important conclusions about the propagation mechanisms. Correlation could come from three effects:

1) each scatterer could induce "wavelength dispersion" by having strongly frequency-dependent reflection/diffraction properties in the considered band;

2) the delay of a scatterer could lie at the boundary of two adjacent bins even after the delay-axis translation described in Section III; or
3) the uncorrelated scattering (US) assumption [33] could be violated.

Since the correlation coefficients are very small, we conclude that none of those three effects has a marked impact.

Before describing the statistical model in Section IV, we summarize our findings of the data analysis as follows. The average energy gains $\overline{G}_k$ vary both with the excess delay and the large-scale conditions, while the m_k parameters depend only on the excess delay.[11] Given the $\overline{G}_k$ and the m_k, the normalized energy gain of the MPCs arriving in the same room at different excess delays are independent realizations of the gamma distribution $\Gamma(\overline{G}_k; m_k)$.

IV. The Statistical Model

A. Modeling Philosophy

As in any wireless channel, the received signal is a sum of the replicas (echoes) of the transmitted signal, being related to the reflecting, scattering, and/or deflecting objects via which the signal propagates. Each of the echoes is related to a single such object. There is, however, one major difference between UWB and narrowband system: in a narrowband system, the echoes at the receiver are only attenuated, phase-shifted and delayed, but undistorted, so that the received signal may be modeled as a linear combination of N_{path} delayed basic waveforms $w(t)$

$$r(t) = \sum_{i=1}^{N_{\text{path}}} c_i w(t-\tau_i) + n(t) \tag{5}$$

where $n(t)$ is the observation noise.

In UWB systems, the frequency selectivity of the reflection, scattering, and/or diffraction coefficients of the objects via which the signal propagates, can lead to a distortion of the transmitted pulses. Furthermore, the distortion and, thus, the shape of the arriving echoes, varies from echo to echo. The received signal is, thus, given as

$$r(t) = \sum_{i=1}^{N_{\text{path}}} c_i \tilde{w}_i(t-\tau_i) + n(t). \tag{6}$$

If the pulse distortion was greater than the width of the delay bins (2 ns), one would observe a significant correlation between adjacent bins. The fact that the correlation coefficient remains very low for all analyzed set of the data implies that the distortion of a pulse due to a single echo is not significant, so that in the following, (5) can be used.

B. Relation Between Parameters

The SSA-PDP of the channel may be expressed as

$$\overline{g}(\tau) = \sum_{k=1}^{N_{\text{bins}}} \overline{G}_k \delta(\tau-\tau_k) \tag{7}$$

where the function $\overline{g}(\tau)$ can be interpreted as the average energy received at a certain receiver position and a delay τ, normalized to the total energy received at one meter distance, and N_{bins} is the total number of bins in the observation window. Assuming an exponential decay starting from the second bin, we have

$$\overline{g}(\tau) = \overline{G}_1 \delta(\tau-\tau_1) + \sum_{k=2}^{N_{\text{bins}}} \overline{G}_2 \exp[-(\tau_k-\tau_2)/\varepsilon] \delta(\tau-\tau_k) \tag{8}$$

where ε is the decay constant of the SSA-PDP.

The total average energy received over the observation interval T is

$$\overline{G}_{\text{tot}} = \int_0^T \overline{g}(\tau)\, d\tau = \overline{G}_1 + \sum_{k=2}^{N_{\text{bins}}} \overline{G}_2 \exp[-(\tau_k-\tau_2)/\varepsilon]. \tag{9}$$

Summing the geometric series, we obtain

$$\overline{G}_{\text{tot}} = \overline{G}_1[1 + rF(\varepsilon)] \tag{10}$$

where $r = \overline{G}_2/\overline{G}_1$ is the power ratio, and

$$F(\varepsilon) = \frac{1-\exp[-(N_{\text{bins}}-1)\Delta\tau/\varepsilon]}{1-\exp(-\Delta\tau/\varepsilon)} \simeq \frac{1}{1-\exp(-\Delta\tau/\varepsilon)}. \tag{11}$$

The total normalized average energy is lognormally distributed, due to the shadowing, around the mean value given from the path loss model (1)

$$\overline{G}_{\text{tot}} \sim \mathcal{L}_{\mathcal{N}}(-PL; 4.3) \tag{12}$$

Inverting (10), we obtain the average energy gains as

$$\overline{G}_k = \begin{cases} \dfrac{\overline{G}_{\text{tot}}}{1+rF(\varepsilon)}, & \text{for } k=1 \\ \dfrac{\overline{G}_{\text{tot}}}{1+rF(\varepsilon)}\, r e^{-((\tau_k-\tau_2)/\varepsilon)}, & \text{for } k=2, \ldots, N_{\text{bins}} \end{cases} \tag{13}$$

and (7) may be rewritten as

$$\overline{g}(\tau) = \frac{\overline{G}_{\text{tot}}}{1+rF(\varepsilon)} \cdot \left\{ \delta(\tau-\tau_1) + \sum_{k=2}^{N_{\text{bins}}} \left[r e^{-((\tau_k-\tau_2)/\varepsilon)} \right] \delta(\tau-\tau_k) \right\}. \tag{14}$$

C. Implementation Recipe

In our model, the local PDP is fully characterized by the pairs $\{G_k, \tau_k\}$, where $\tau_k = (k-1)\Delta\tau$ with $\Delta\tau = 2$ ns. The G_k are generated by a superposition of large and small-scale statistics.

We start out by generating the total mean energy $\overline{G}_{\text{tot}}$ at a certain distance according to (12). Next, we generate the decay constant ε and the power ratio r as lognormal distributed random numbers

$$\varepsilon \sim \mathcal{L}_{\mathcal{N}}(16.1; 1.27) \tag{15}$$

$$r \sim \mathcal{L}_{\mathcal{N}}(-4; 3). \tag{16}$$

We set the width of the observation window to be $T = 5\varepsilon$. Thus, the SSA-PDP is completely specified according to (14). Finally, we generate the local PDPs by computing the normalized energy

[11] Future refinements of the model could include spatial coherence lengths for the $\overline{G}_k$'s and m_k's, as well as a possible distance dependence of the m_k's.

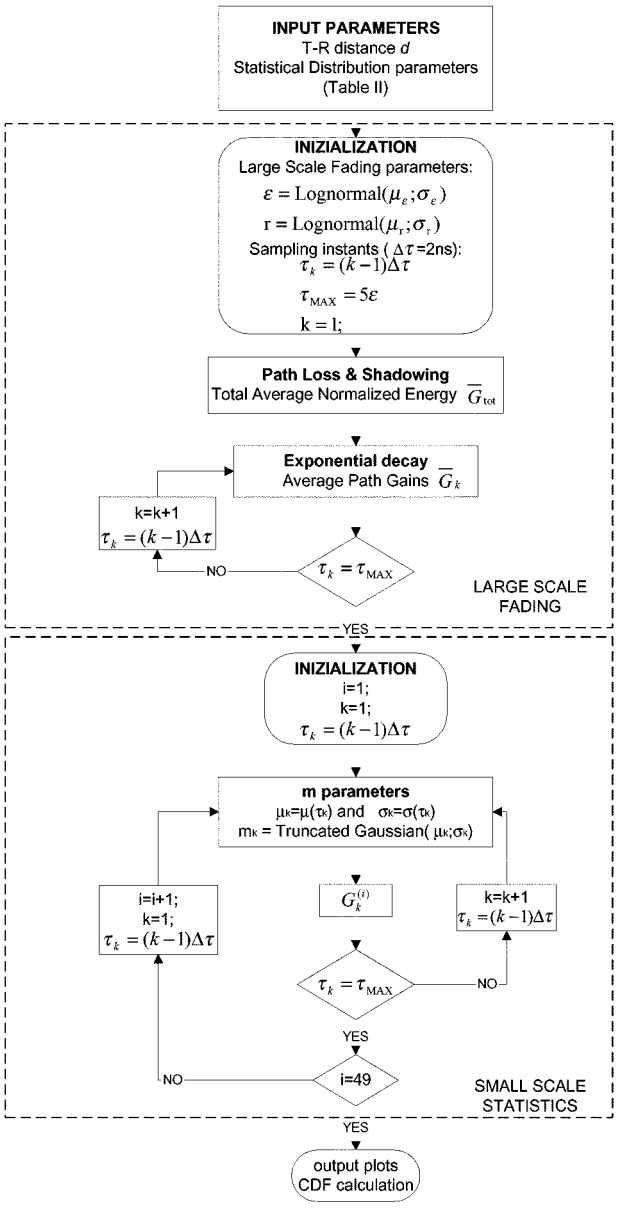

Fig. 12. The flowchart of the simulation procedure.

gains $G_k^{(i)}$ of every bin k and every location i as Gamma distributed independent variables. The Gamma distributions have the average given by (13), and the m_k's are generated as independent truncated Gaussian random variables

$$m_k \sim \mathcal{T}_{\mathcal{N}}(\mu_m(\tau_k);\, \sigma_m^2(\tau_k)) \tag{17}$$

with $\mu_m(\tau_k)$ and $\sigma_m^2(\tau_k)$ given by (3) and (4).

The computer implementation is summarized in the flowchart of Fig. 12; the statistical models and required parameters are shown in Table II. Small changes in the receiver position result in different local PDPs, corresponding to different realizations of the local energy gains G_k's, whereas the SSA-PDP does not change. When the changes of the receiver position are such that the environment changes as well, the SSA-PDP should be generated according to the new large-scale conditions, and the local PDPs are generated about the new SSA-PDP.

TABLE II
STATISTICAL MODELS AND PARAMETERS

GLOBAL PARAMETERS $\Rightarrow \overline{G}_{\text{tot}}$ and $\overline{G}_k$	
Path Loss	$PL = \begin{cases} 20.4 \cdot \log_{10}(d/d_0) & d \le 11\text{m} \\ -56 + 74 \cdot \log_{10}(d/d_0) & d > 11\text{m} \end{cases}$
Shadowing	$\overline{G}_{\text{tot}} \sim \mathcal{L}_{\mathcal{N}}(-PL;\, 4.3)$
Decay Constant	$\varepsilon \sim \mathcal{L}_{\mathcal{N}}(16.1; 1.27)$
Power Ratio	$r \sim \mathcal{L}_{\mathcal{N}}(-4;\, 3)$
LOCAL PARAMETERS $\Rightarrow G_k$	
Energy Gains	$G_k \sim \Gamma(\overline{G}_k;\, m_k)$
m values	$m_k \sim \mathcal{T}_{\mathcal{N}}(\mu_{\text{m}}(\tau_k);\, \sigma_{\text{m}}^2(\tau_k))$ $\mu_{\text{m}}(\tau_k) = 3.5 - \frac{\tau_k}{73}$ $\sigma_{\text{m}}^2(\tau_k) = 1.84 - \frac{\tau_k}{160}$

V. SIMULATION EXAMPLES

In this section, we will first present the results obtained from 49 simulated multipath profiles, generated based on the statistical model described above, in which the local variables are changed according to the small-scale statistics, and the "global" variables such as the total averaged received energy $\overline{G}_{\text{tot}}$, the decay constant ε, and the power ratio r are fixed. Our aim is to reproduce the small-scale statistics over the 49 locations on the grid. Note that measured multipath profiles that are influenced by small-scale effects, also may be influenced possibly by the large-scale effects even if the profiles are obtained within one room, i.e., among the 49 points of a measurement grid. Such a situation could occur if some positions on the grid experience different illumination conditions from the transmitter, i.e., different shadowing for different subsets of the 49 points, e.g., due to the presence of a door or metal filing cabinet.

Figs. 13 and 14 show an exemplary set of experimental and simulated local PDPs. The 49 simulated local PDPs are generated assuming the same distance from the transmitter where the exemplary set of multipath profiles were measured. The parameters related to the large-scale statistics (i.e., the total averaged received energy $\overline{G}_{\text{tot}}$, the decay constant ε, and the power ratio r) were set equal to the corresponding parameters extracted from the measurement data of that particular room. Since the comparison is done between statistical realizations, the agreement can be evaluated only qualitatively. It is evident from Figs. 13 and 14 that the simulated and the measured PDPs do agree in that sense.

By integrating each local PDPs over all delay bins, we define the signal quality as the ratio of the total averaged energy received at a given T–R separation distance and total energy received at the reference distance of one meter. For each room, we then obtain the cumulative distribution function (CDF) of the signal quality using 49 local PDPs over the measurement grid. We found that the simulated CDFs tend to be slightly narrower than the experimental ones. This is apparent in Fig. 15, which

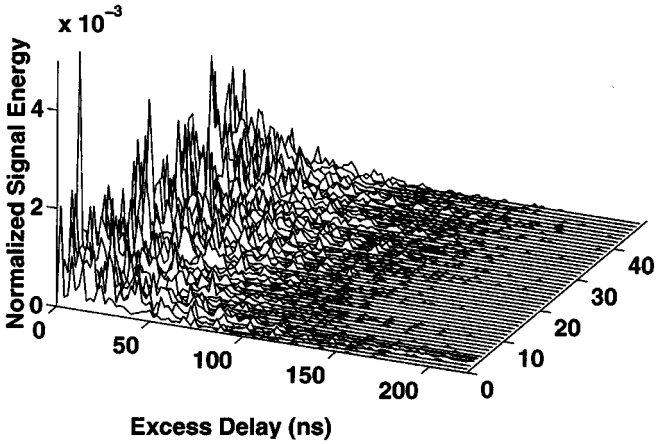

Fig. 13. The measured 49 local PDPs for an exemplary room.

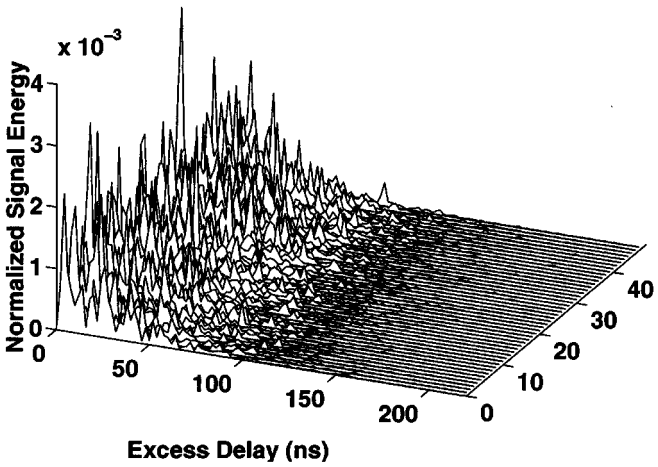

Fig. 14. Simulated 49 local PDPs for an exemplary room.

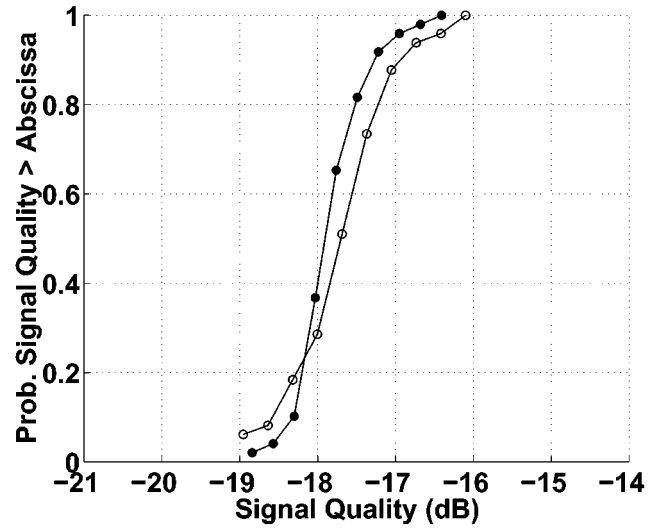

Fig. 15. Comparison between the measured and simulated CDF of the signal quality received in an exemplary room. The circles represent the experimental data, and the dots represent the simulation results.

shows the empirical and simulated CDFs of an exemplary room. A possible explanation for this behavior is that the experimental CDFs may be affected, partially, by the large-scale statistics, in the sense that the illumination conditions of the 49 points of the grid may be different. Such effect of the large-scale statistics tends to spread the intensity distribution of the 49 points.

Furthermore, in the simulations we noted that, as a general trend, small values of the decay constant ε correspond to a large spread of the associated CDFs. This result can be easily explained as follows. The spread of the CDF of the signal quality is related to the spread of the energy due to small-scale fading. The obtained total energy is the sum of the energies in the different bins, i.e., a sum over a large number of independent, Gamma distributed, random variables. As the bin width is independent of ε, the diversity order (i.e., the effective number of independent variables) is smaller for smaller decay constant ε, producing larger relative fluctuations of the total received energy.

VI. Conclusion

We performed a statistical analysis of UWB channel data, obtained from an extensive measurement campaign in a typical modern office environment. Based on this analysis, we proposed a statistical model of a UWB propagation channel. The actual parameter values extracted from the measurements may be specific for this building. However, the methodology and the model setup is general, and can be easily applied to future measurement campaigns.

Our results cannot rule out the presence of distorted replicas of the elementary received waveforms in the PDP. The arrival times of these replicas may be periodical because of multiple reflections. Manifestation of the detection of these periodic replicas could be the narrow, equally spaced lines that are ubiquitous in the spectra of the detected PDPs. This is a point, however, that deserves further investigation.

The analysis of UWB channel data, however, shows that the well-established tapped-delay-line model, with independent fading of the taps (bins), accurately reproduces the behavior of the measured channel. In contrast to narrowband models, the energy statistics due to small-scale effects follow a Gamma distribution for *all* bins, with the m factor decreasing with increasing excess delay. The variations of the large-scale parameters, such as the total averaged energy, decay constant, and ratio of the energies in the first and second bin, can be modeled as stochastic parameters that change, e.g., from room to room. Statistical distributions of all involved parameters were obtained.

With this model, accurate performance predictions of UWB spread spectrum systems become feasible. In future work, we plan to apply our model to UWB system simulations and analyze the sensitivity of system performance to various transmission parameters.

Acknowledgment

The authors would like to thank the anonymous reviewers and the Guest Editor for their helpful comments, especially for suggesting us to include the review of the propagation experiment which provided for a more self-contained paper. They wish to acknowledge L. J. Greenstein, T. M. Willis, J. H. Winters, and L. A. Shepp for helpful discussions.

The work was performed during visits of D. Cassioli and A. Molisch at AT&T Labs–Research. The authors also wish to thank F. Vatalaro, E. Bonek, W. Leeb, B. Tkach, and T. Darcie for providing a research environment where collaborations such as this are possible.

REFERENCES

[1] M. Z. Win and R. A. Scholtz, "Impulse radio: How it works," *IEEE Commun. Lett.*, vol. 2, pp. 36–38, Feb. 1998.

[2] M. Z. Win, X. Qiu, R. A. Scholtz, and V. O. Li, "ATM-based TH-SSMA network for multimedia PCS," *IEEE J. Select. Areas Commun.*, vol. 17, pp. 824–836, May 1999.

[3] M. Z. Win and R. A. Scholtz, "Ultra-wide bandwidth time-hopping spread-spectrum impulse radio for wireless multiple-access communications," *IEEE Trans. Commun.*, vol. 48, pp. 679–691, Apr. 2000.

[4] R. A. Scholtz, R. Weaver, E. Homier, J. Lee, P. Hilmes, A. Taha, and R. Wilson, "UWB radio deployment challenges," in *Proc. IEEE Int. Symp. Personal, Indoor, Mobile Radio Communications*, vol. 1, London, U.K., Sept. 2000, pp. 620–625.

[5] H. Luediger and S. Zeisberg, "User and business perspective on an open mobile access standard," *IEEE Commun. Mag.*, vol. 38, pp. 160–163, Sept. 2000.

[6] J. Conroy, J. L. LoCicero, and D. R. Ucci, "Communication techniques using monopulse waveforms," in *Proc. Military Communications Conf.*, Atlantic City, NJ, Oct. 1999, pp. 1181–1185.

[7] G. D. Weeks, J. K. Townsend, and J. A. Freebersyser, "Performance of hard decision detection for impulse radio," in *Proc. Military Communications Conf.*, Atlantic City, NJ, Oct. 1999, pp. 1201–1206.

[8] H. Lee, B. Han, Y. Shin, and S. Im, "Multipath characteristics of impulse radio channels," in *Proc. 50th Annual Int. Vehicular Technology Conf.*, Tokyo, Japan, 2000, pp. 2487–2491.

[9] C. J. Le Martret and G. B. Giannakis, "All-digital PAM impulse radio for multiple-access through frequency-selective multipath," in *Proc. IEEE Global Telecomm. Conf.*, Nov. 2000, pp. 77–81.

[10] M.-S. Alouini, A. Scaglione, and G. Giannakis, "PCC: Principal components combining for dense correlated multipath fading environments," in *Proc. IEEE Semiannu. Vehicular Technology Conf.*, Boston, MA, Sept. 2000, pp. 2510–2517.

[11] J. R. Foerster, "The effects of multipath interference on the performance of UWB systems in an indoor wireless channel," in *Proc. IEEE Semiannual Vehicular Technology Conf.*, Rhodos, Greece, May 2001, pp. 1176–1180.

[12] X. Huang and Y. Li, "Generating near-white ultra-wideband signals with period extended PN sequences," in *Proc. IEEE Semiannual Vehicular Technology Conf.*, vol. 2, Rhodos, Greece, May 2001, pp. 1184–1188.

[13] M. L. Welborn, "System considerations for ultra-wideband wireless networks," in *Proc. IEEE Radio and Wireless Conf.*, Boston, MA, Aug. 2001, pp. 5–8.

[14] J. D. Taylor, Ed., *Introduction to Ultra-Wideband Radar Systems*, 1st ed. Boca Ranton, FL: CRC, 1995.

[15] M. Z. Win and R. A. Scholtz, "On the robustness of ultra-wide bandwidth signals in dense multipath environments," *IEEE Commun. Lett.*, vol. 2, pp. 51–53, Feb. 1998.

[16] ——, "On the energy capture of ultra-wide bandwidth signals in dense multipath environments," *IEEE Commun. Lett.*, vol. 2, pp. 245–247, 1998.

[17] M. Z. Win and Z. A. Kostić, "Virtual path analysis of selective Rake receiver in dense multipath channels," *IEEE Commun. Lett.*, vol. 3, pp. 308–310, Nov. 1999.

[18] M. Z. Win, G. Chrisikos, and N. R. Sollenberger, "Performance of Rake reception in dense multipath channels: Implications of spreading bandwidth and selection diversity order," *IEEE J. Select. Areas Commun.*, vol. 18, pp. 1516–1525, Aug. 2000.

[19] M. Z. Win and G. Chrisikos, "Impact of spreading bandwidth and selection diversity order on selective Rake reception," in *Wideband Wireless Digital Communications, Invited Chapter*, A. F. Molisch, Ed. Upper Saddle River, NJ: Prentice-Hall, 2001.

[20] A. A. Saleh and R. A. Valenzuela, "A statistical model for indoor multipath propagation," *IEEE J. Select. Areas Commun.*, vol. 5, pp. 128–137, Feb. 1987.

[21] T. S. Rappaport, S. Y. Seidel, and K. Takamizawa, "Statistical channel impulse response models for factory an open plan building radio communication system design," *IEEE Trans. Commun.*, vol. 39, pp. 794–807, May 1991.

[22] H. Hashemi, "The indoor radio propagation channel," *Proc. IEEE*, vol. 81, pp. 943–968, July 1993.

[23] ——, "Impulse response modeling of indoor radio propagation channels," *IEEE J. Select. Areas Commun.*, vol. 11, pp. 967–978, Sept. 1993.

[24] M. Z. Win, R. A. Scholtz, and M. A. Barnes, "Ultra-wide bandwidth signal propagation for indoor wireless communications," in *Proc. IEEE Int. Conf. Communication*, vol. 1, Montréal, QC, Canada, June 1997, pp. 56–60.

[25] M. Steinbauer and A. F. Molisch, "Directional channel models," in *Flexible Personalized Wireless Communications*, L. M. Correia, Ed. New York: Wiley, 2001, ch. 3.2.

[26] H. Hashemi, "Simulation of the urban radio propagation channel," *IEEE Trans. Veh. Technol.*, vol. VT-28, pp. 213–225, Aug. 1979.

[27] A. F. Molisch and M. Steinbauer, "Condensed parameters for characterizing wideband mobile radio channels," *Int. J. Wireless Inform. Networks*, vol. 6, pp. 133–154, July 1999.

[28] L. J. Greenstein, V. Erceg, Y. S. Yeh, and M. V. Clark, "A new path-gain/delay-spread propagation model for digital cellular channels," *IEEE Trans. Veh. Technol.*, vol. 46, pp. 477–485, May 1997.

[29] V. Erceg, L. J. Greenstein, S. Y. Tjandra, S. R. Parkoff, A. Gupta, B. Kulic, A. A. Julius, and R. Bianchi, "An empirically based path loss model for wireless channels in suburban environments," *IEEE J. Select. Areas Commun.*, vol. 17, pp. 1205–1211, July 1999.

[30] E. Failli, Ed., *Digital Land Mobile Radio. Final Report of COST 207*. Luxemburg: Commission of the European Union, 1989.

[31] M. Nakagami, "The m-distribution—A general formula of intensity distribution of rapid fading," in *Statistical Method in Radio Wave Propagation*, W. C. Hoffman, Ed. Oxford, U.K.: Pergamon, 1960, pp. 3–36.

[32] W. R. Braun and U. Dersch, "A physical mobile radio channel model," *IEEE Trans. Veh. Technol.*, vol. 40, pp. 472–482, May 1991.

[33] P. A. Bello, "Characterization of randomly time-variant linear channels," *IEEE Trans. Commun. Syst.*, vol. COM–11, pp. 360–393, Dec. 1963.

Dajana Cassioli (S'02) received the "Laurea" degree in electronic engineering from the University of Rome "Tor Vergata," Rome, Italy, in 1999. She is currently at the Electronic Engineering Department of the University of Rome Tor Vergata, working toward her Ph.D. degree.

From 1998 to 1999, she was with the Fondazione Ugo Bordoni, Rome, where she was involved in the study of semiconductor optical amplifiers and in the development of computer models of devices for WDM optical communication systems. In 1999, she joined the Communication Group of the Electronic Engineering Department of the University of Rome "Tor Vergata," where she has been involved in the analysis and simulation of the TD-CDMA radio interface of the UMTS system. Her main research interests are in the field of wireless access technologies, and in particular of the UWB radio technology, ad hoc networks and Bluetooth. In the summer of 2000, she was a visitor with the Wireless Systems Research Department at AT&T Labs–Research, Red Bank, NJ, working on the statistical analysis of UWB signal propagation. She is also the Project Manager of the UWB technology research activity of RadioLabs, a Consortium between the Electronics Engineering Department of the University of Rome "Tor Vergata" and an Italian company operating in the field of wireless communications.

Moe Z. Win (S'85–M'87–SM'97) received the B.S. degree (*magna cum laude*) from Texas A&M University, College Station, and the M.S. degree from the University of Southern California (USC), Los Angeles, in 1987 and 1989, respectively, in electrical engineering. As a Presidential Fellow at USC, he received both the M.S. degree in applied mathematics and the Ph.D. degree in electrical engineering, in 1998.

In 1987, he joined the Jet Propulsion Laboratory (JPL), California Institute of Technology, Pasadena. From 1994 to 1997, he was a Research Assistant with the Communication Sciences Institute at USC, where he played a key role in the successful creation of the Ultra-Wideband Radio Laboratory. Since 1998, he has been with the Wireless Systems Research Department, AT&T Laboratories–Research, Middletown, NJ, where he is a Principal Technical Staff Member. His main research interests are the application of communication, detection, and estimation theories to a variety of communications problems including time-varying channels, diversity, equalization, synchronization, signal design, ultra-wide-bandwidth communication, and optical communications.

Dr. Win is a member of Eta Kappa Nu, Tau Beta Pi, Pi Mu Epsilon, Phi Theta Kappa, and Phi Kappa Phi. He was a University Undergraduate Fellow at Texas A&M University, where he received, among others awards, the Academic Excellence Award. At USC, he received several awards including the Outstanding Research Paper Award and the Phi Kappa Phi Student Recognition Award. He was the recipient of the IEEE Communications Society Best Student Paper Award at the Fourth Annual IEEE NetWorld+Interop'97 Conference. He has been involved actively in chairing and organizing sessions and has served as a member of the Technical Program Committee in a number of IEEE conferences. He currently serves as the Technical Program Chair for the IEEE Communication Theory Symposium of ICC-2004 the Technical Program Chair for and IEEE Conference on Ultra Wideband Systems and Technologies (2002); and Technical Program Vice-Chair for IEEE International Conference on Communications (2002). He served as the Tutorial Chair for IEEE Semiannual International Vehicular Technology Conference (Fall-2001) and the Technical Program Chair for the IEEE Communication Theory Symposium of Globecom-2000. He is the current Editor for *Equalization and Diversity* for the IEEE TRANSACTIONS ON COMMUNICATIONS and a Guest Editor for the 2002 IEEE JOURNAL ON SELECTED AREAS IN COMMUNICATIONS, Special Issue on Ultra Wideband Radio in Multiaccess Wireless Communications.

Andreas F. Molisch (S'89–M'95–SM'00) received the Dipl.Ing., Dr.Techn., and Habilitation degrees from the Technical University (TU) Vienna, Austria, in 1990, 1994, and 1999, respectively.

From 1991 to 2001, he was with the Institut fuer Nachrichtentechnik und Hochfrequenztechnik (INTHFT) of the TU Vienna, becoming an Associate Professor there in 1999. From 1999 to 2000, he was on leave to the FTW Research Center for Telecommunications, Vienna. Since March 2001, he has been with the Wireless Systems Research Department at AT&T Laboratories–Research, Middletown, NJ. He has done research in the areas of SAW filters, radiative transfer in atomic vapors, atomic line filters, and base station antennas. His current research interests are the measurement and modeling of mobile radio channels, MIMO systems, smart antennas, and wideband wireless systems. He has authored, coauthored, or edited two books, five book chapters, some 50 journal papers, and numerous conference contributions.

Dr. Molisch is an Editor of the IEEE TRANSACTIONS ON WIRELESS COMMUNICATIONS and Co-Editor of an upcoming special issue on MIMO and Smart Antennas in *Journal of Wireless Communications Mobile Computing*. He has participated in the European research initiatives "COST 231," "COST 259," and "COST273," where he is chairman of the MIMO channel modeling subgroup. He received the GIT prize of the Austrian Electrical Engineering Society, in 1991, the Kardinal Innitzer prize for Best Engineering Habilitation Thesis, in 1999, and an INGVAR Award of the Swedish Strategic Research Foundation, in 2001. He has also been Session Organizer, Session Chairman, and Member of the Program Committee at various international conferences.